Hydrophobicity Scaling of Aqueous Interfaces by an Electrostatic Mapping

Richard C. Remsing[1,2] and John D. Weeks[1,a)]
[1)] *Institute for Physical Science and Technology, Department of Chemistry and Biochemistry, and Chemical Physics Program, University of Maryland, College Park, MD 20742*
[2)] *Department of Chemical and Biomolecular Engineering, University of Pennsylvania, Philadelphia, PA 19104*[b)]

An understanding of the hydrophobicity of complex heterogenous molecular assemblies is crucial to characterize and predict interactions between biomolecules. As such, uncovering the subtleties of assembly processes hinges on an accurate classification of the relevant interfaces involved, and much effort has been spent on developing so-called "hydrophobicity maps." In this work, we introduce a novel electrostatics-based mapping of aqueous interfaces that focuses on the collective, long-wavelength electrostatic response of water to the presence of nearby surfaces. In addition to distinguishing between hydrophobic and hydrophilic regions of heterogenous surfaces, this electrostatic mapping can also differentiate between hydrophilic regions that polarize nearby waters in opposing directions. We therefore expect this approach to find use in predicting the location of possible water-mediated hydrophilic interactions, in addition to the more commonly emphasized hydrophobic interactions that can also be of significant importance.

Keywords: Protein Hydration, Hydropathy Scales, Self Assembly, Polarization, Dielectric Response, Hydrogen Bonding

arXiv:1502.05587v1 [cond-mat.soft] 19 Feb 2015

I. INTRODUCTION

The formation of complex mesoscopic structures is generally driven by the self assembly of nanoscale building blocks. Oftentimes, the assembly of individual units into a larger complex is driven by strong, direct interactions between the chemical constituents[1–4]. In many cases, however, the assembly of molecular building blocks is triggered by the solvent and not by direct interactions between the individual units. For example, water-mediated interactions between nonpolar entities, known as hydrophobic effects[5,6], induce the folding of proteins by minimizing the contact area between hydrophobic amino acid residues and water at the surface of the protein[7–10]. Both hydrophobic and electrostatic interactions are also thought to play a role in protein-protein binding processes[2,11,12]. Driven by such applications, many researchers have proposed empirical hydrophobicity scales for characterizing and predicting the relative hydrophobicity of complex surfaces. In general, these approaches fall into one of two classes, *surface-based* and *water-based* hydrophobicity scales.

Surface-based hydrophobicity scales[13–16] seek to predict the relative hydrophobicity of a water-surface interface from the properties of the surface alone. Such mappings have generally been used to predict the properties of proteins and other complex biological surfaces. Classic hydrophobicity scales like the Kyte-Doolittle scale[13] assign a value of relative hydrophobicity to each macromolecular building block or residue.

Another residue-based scale was introduced by Berne and coworkers to characterize the binding regions of protein surfaces involved in protein-protein interactions, and hundreds of surfaces were examined to predict if a dewetting transition could occur upon protein complex formation[15]. This analysis indeed successfully uncovered several binding processes in which a dewetting transition was likely to occur, as confirmed by molecular dynamics simulations with explicit water molecules[15].

More recent approaches have demonstrated that incorporation of atomic-level details may provide an even better characterization of surfaces than classifying an entire residue as hydrophobic or hydrophilic. In particular, Kapcha and Rossky (KR) have exploited the assignment of partial charges in atomistic models of proteins to classify individual atomic units as hydrophobic or hydrophilic on a binary scale[16]. Predictions from these KR maps are in much better agreement with more detailed results than those from residue-based methods and have been used to characterize a wide range of protein surfaces and binding pockets[16].

Despite these predictive successes, surface-based hydrophobicity scales only implicitly account for the influence of surface topography and the chemistry of nearby atomic units on the hydrogen bond network of water. In light of these limitations, new methods have been developed for providing a direct characterization of the nonlocal response of water to complex material surfaces. In particular, recent work has focused on the nature of density fluctuations in bulk water and at aqueous interfaces[17–23].

Density fluctuations are intimately related to solvation thermodynamics through potential distribution theory, which can be used to relate the solvation free energy of a hard object to the probability of observing a cavity or volume of equal shape and size being empty[24–27]. A large cavity or extended hydrophobic surface disrupts the hydrogen bond network and density fluctuations are enhanced relative to those in the bulk or near a hydrophilic surface. This disruption of the network is the key physi-

[a)] jdw@umd.edu
[b)] rremsing@seas.upenn.edu

cal feature characterizing large scale hydrophobic effects, and this makes it easier to create a cavity near a hydrophobic surface than a hydrophilic one. Previous work has exploited this fact, and used the solvation free energy of hard shaped objects or cavities near a surface as a measure of its hydrophobicity[17–23].

Because this approach focuses on the response of water to a substrate, density fluctuation-based mappings can account for both chemical and topographical complexities of a surface. However performing such calculations, especially for large asymmetric volumes, can be computationally intense, often requiring several simulations with advanced umbrella-sampling techniques to obtain the solvation free energy of a single volume. Moreover, this type of mapping depends on the size, shape, and position of the probe volume to be emptied and in the absence of a general theory, different choices can lead to ambiguities in the estimate of hydrophobicity. While fluctuation methods very successfully discriminate between hydrophobic and hydrophilic surfaces, little distinction is seen between surfaces with similar hydrophilicity but different chemistries.

In this work, we introduce a simple approach to characterize chemically and topographically complex materials based on the collective, long-wavelength electrostatic response of water to such surfaces. Excluded volume constraints and the partial surface charges exploited in the KR scale can produce distortions and disruptions of the hydrogen bond network. Extended hydrophobic regions can break hydrogen bonds, while polar regions can locally distort and pin bonds in the network. This complicated nonlocal response rearranges the molecular dipoles in water and is encoded in the electrostatic potential.

As we will see, the long-wavelength component of the induced potential readily distinguishes between hydrophobic and hydrophilic surfaces, and also provides additional insight into the net polarization of water at a polar interface. This is used to differentiate between hydrophilic surfaces with similar contact angles but different chemical structures. We anticipate that this computationally simple method of analysis, which requires only a single equilibrium simulation, will find use as a tool to efficiently characterize complex surfaces with nanoscale chemical and topographical patterning, like the surface of proteins involved in complex formation. However, the forces generating the distortions of the hydrogen bond network are by no means purely electrostatic, and direct physical connections to macroscopic measurements of hydrophobicity like the contact angle or the solvation free energy of cavities will require more general treatments.

II. ELECTROSTATIC RESPONSE AT UNIFORM PLANAR SURFACES

We first introduce our approach and its underlying concepts through the study of uniform planar surfaces with varying hydrophobicity. In particular, we study the response of water to the model atomically-detailed and corrugated silica-like surfaces of Giovambattista, Rossky, and Debenedetti[28,29]. These artificial surfaces are dipolar, with the dipole moment of surface groups created by negative partial charges placed on the uppermost layer of oxygen sites and positive charges on the subsequent layer of silicon atoms. In order to tune the relative polarity of the surface, the magnitude of the atomic charges, q, is linearly coupled to a parameter ξ, such that the dipole moment of each surface unit is given by $\xi\mathbf{p} = (0, 0, \xi q d_{\mathrm{OSi}})$, where d_{OSi} is the oxygen-silicon bond length. A nonpolar, hydrophobic surface with a contact angle of $\theta_\xi \approx 109°$ is obtained when $\xi = 0$. Increasing the magnitude of ξ leads to an increase in the hydrophilicity of the surface, as characterized by a decrease in the contact angle θ_ξ, and there is a slight asymmetry with respect to the sign of ξ. For example, $\theta_1 \approx 90°$, while $\theta_{-1} \approx 85°$[28,29].

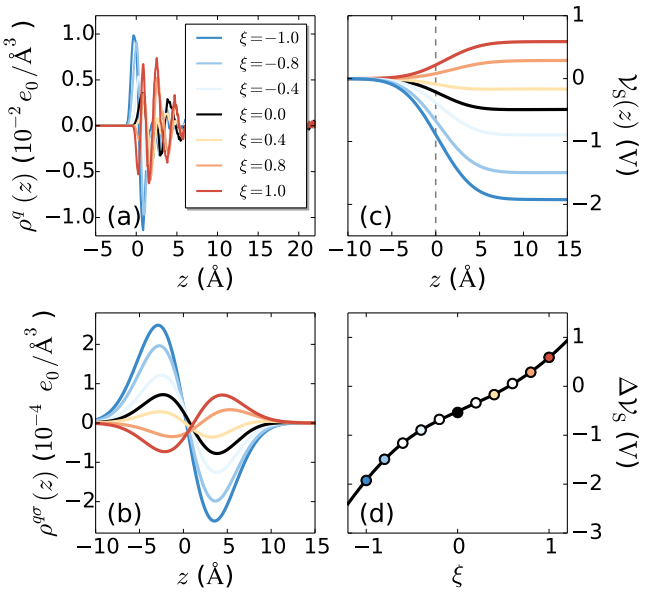


FIG. 1. (a) Bare charge densities provide little information about the collective electrostatic response of water to model silica surfaces of varying polarity, ξ. (b) Upon Gaussian-smoothing, however, a long-ranged, collective dipole layer at the interface is apparent. This dipole layer characterizes the response of water to the polarity of the surface. (c) The Gaussian-smoothed electrostatic potential due to water provides a slowly varying metric quantifying this interfacial dipole layer. (d) The difference $\Delta\mathcal{V}_S$ in the long-ranged electrostatic potential in bulk water and in the effective vacuum inside the silica surface, or at the surface itself as indicated by the dashed line, characterizes the nonlinear response of water to the magnitude of the dipole of the surface.

In Figure 1a, we show $\rho^q(z)$, the variation in the z-direction of the bare charge density of water,

$$\rho^q(\mathbf{r}) \equiv \left\langle \sum_i^{N_C} q_i \delta(\mathbf{r} - \mathbf{r}_i(\overline{\mathbf{R}})) \right\rangle, \qquad (1)$$

where the sum is over all N_C charged sites with charge

q_i and position $\mathbf{r}_i(\overline{\mathbf{R}})$ in configuration $\overline{\mathbf{R}}$, and $\langle\cdots\rangle$ indicates an ensemble average over all configurations and we have averaged over the remaining two coordinates in $\mathbf{r}$. Because of the rapidly varying molecular scale surface structure and charge distributions, little insight into the collective response of water to the surface is garnered from $\rho^q(z)$, and an alternative description of the ordering of interfacial water is needed.

A clearer measure of the long-wavelength electrostatic response of water induced by a heterogeneity is given by the Gaussian-smoothed charge density $\rho^{q\sigma}(\mathbf{r})$ that naturally arises within the context of the local molecular field (LMF) theory of electrostatics[30]. Here

$$\rho^{q\sigma}(\mathbf{r}) = \int d\mathbf{r}'\rho^q(\mathbf{r}')\rho_G(|\mathbf{r}-\mathbf{r}'|), \tag{2}$$

$\rho_G(\mathbf{r})$ is a normalized Gaussian function given by

$$\rho_G(\mathbf{r}) = \frac{1}{\pi^{3/2}\sigma^3} e^{-\left(\frac{|\mathbf{r}|^2}{\sigma^2}\right)}, \tag{3}$$

and σ is a smoothing length used to average over short-ranged rapidly varying components of the electrostatic interactions. Previous work has shown that useful smoothing results when σ is chosen on the order of nearest-neighbor distances[30–32], and we choose $\sigma = 4.5$ Å herein. This type of smoothing over molecular sizes, often discussed in elementary electrostatic texts[33,34], washes out the effects of atomic-scale details, and it has been argued that $\rho^{q\sigma}(\mathbf{r})$ provides a good qualitative characterization of the underlying long wavelength electrostatic response of fluids[31,32]. Note that in the present case when the bare charge density $\rho^q(\mathbf{r})$ is known directly from simulation, LMF theory is used only to motivate the consideration and usefulness of the smoothed charge density $\rho^{q\sigma}(\mathbf{r})$.

Indeed, as shown in Figure 1b, the Gaussian-smoothed charge densities readily indicate the formation of an interfacial dipole layer arising from subtle changes in the orientation of water molecules near the surface as they are increasingly pinned by the partial charges of the model surface. The formation of a dipole layer is apparent even at the nonpolar surface with $\xi = 0$, as detailed in previous work[31,35,36].

As ξ is increased from zero in the negative direction, this interfacial dipole grows in magnitude. The dominant molecular orientation producing the interfacial dipole for $\xi \ll 0$ corresponds to that sketched in Figure 2c. Here a non-negligible fraction of interfacial water molecules point one O-H bond directly toward the surface, and form hydrogen bonds with the negatively charged "silicon" atoms. The collective interfacial dipole at $\xi = 0$ arises from the smaller fraction of water already existing in this orientation, although most water molecules at the interface then have an orientation where their H-O-H plane is parallel to the surface itself, which makes no contribution to the dipole layer[37].

Conversely, as ξ is increased from zero in the positive direction, the magnitude of the interfacial dipole decreases and eventually changes sign. This is consistent with interfacial water molecules pointing an O-H bond away from the interface with increasing probability as ξ is increased, as evidenced by the probability distributions $P(\theta_{\mathrm{OH}})$ of the angle made by the OH bond vector of a water molecule and the surface normal shown in Figure 2a.

Although the Gaussian-smoothed charge density has provided a physically suggestive description of the response of water to a uniform planar surface, a more quantitative metric is needed to characterize patterned and corrugated surfaces and protein complexes. To that end, we focus attention on $\mathcal{V}_{\mathrm{S}}(\mathbf{r})$, the slowly-varying, long-wavelength portion of the electrostatic potential due to the solvent. This is related to the smoothed charge density $\rho^{q\sigma}(\mathbf{r})$ by Poisson's equation

$$\vec{\nabla}^2\mathcal{V}_{\mathrm{S}}(\mathbf{r}) = -\rho^{q\sigma}(\mathbf{r}), \tag{4}$$

with notation chosen to be consistent with previous work[30]. This potential, shown in Figure 1d, smoothly transitions from zero in the vacuum region well inside the silica surface to a value of $\Delta\mathcal{V}_{\mathrm{S}}$ in the bulk region. Note that trends in $\Delta\mathcal{V}_{\mathrm{S}}$ can be evaluated using other reasonable limits, like the difference between the bulk potential and the dashed line in Figure 1c at the silica surface, without qualitatively affecting the characterization of the interface. We use this fact below when generating an electrostatics-based map of a water-protein interface.

We propose that $\Delta\mathcal{V}_{\mathrm{S}}$ can be utilized as a quantitative measure of the response of water to complex surfaces. Indeed, $\Delta\mathcal{V}_{\mathrm{S}}(\xi)$ shown in Figure 1d quantifies the nonlinear response of the mesoscopic surface dipole layer to changes in ξ, such that the magnitude and sign of water polarization at the surface is captured. Additionally, the relative differences in $\Delta\mathcal{V}_{\mathrm{S}}(\xi)$ are due exclusively to structural rearrangements near the surface (dipolar contributions), because the constant quadrupolar (Bethe potential) contribution to the potential is the same for all ξ-values[38].

Moreover, recent work has emphasized that polar hydrophilic surfaces, which locally pin water molecules, are fundamentally different from nonpolar hydrophilic surfaces that have artificially large Lennard-Jones-like attractions. These latter surfaces simply pull interfacial waters closer to the surface, increasing the contact angle, but do not introduce significant changes in water structure about the position of this interface[39]. Therefore, the local pinning of interfacial waters through polar interactions like hydrogen bonding underlies the hydrophilicity of realistic surfaces, and the electrostatic mapping introduced here captures this behavior.

Finally, we note that in the simple case of a system with a slab-like geometry, the potential difference obtained from the one-dimensional $\mathcal{V}_{\mathrm{S}}(z)$, $\Delta\mathcal{V}_{\mathrm{S}}$, is exactly equal to that estimated from the bare electrostatic potential $\mathcal{V}(z)$, $\Delta\mathcal{V}$. This equality is due to the fact that Gaussian smoothing of the potential conserves the first two nonzero multipole moments of a charge distribution

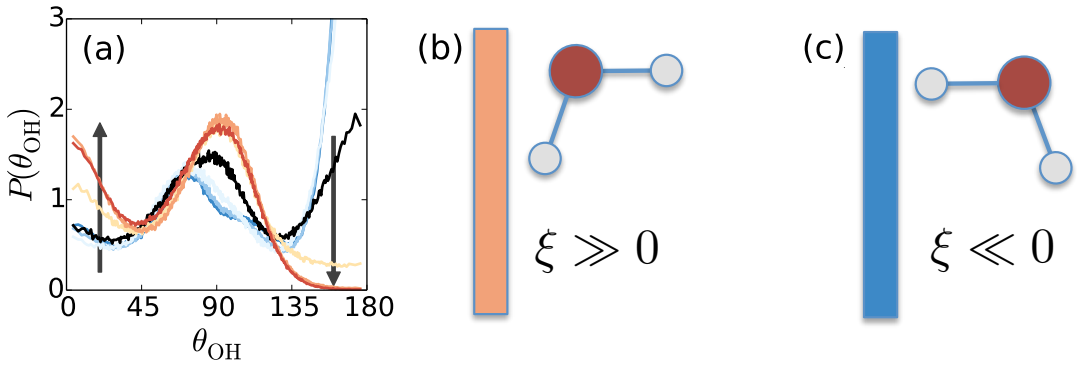


FIG. 2. (a) The probability distribution of the angle made by the surface normal and the OH bond vector, $P(\theta_{\rm OH})$, illustrates that water polarizes differently in response to surfaces with positive and negative ξ. Gray arrows indicate the direction of increasing ξ. (b) For $\xi \gg 0$, interfacial water molecules tend to point an OH bond toward the bulk, while (c) interfacial waters point an OH group toward the surface for $\xi \ll 0$. A small portion of each surface of varying ξ is indicated by the colored rectangle, while the oxygen site is colored red and the hydrogens are colored light gray.

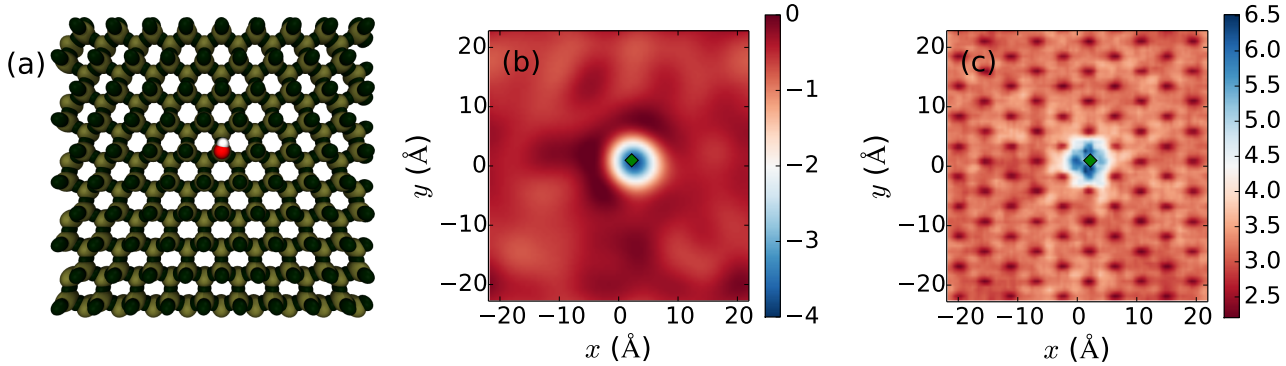


FIG. 3. (a) An otherwise apolar silica surface, composed of oxygen (green) and silicon (yellow) atoms, is patterned with a single, hydrophilic hydroxyl group, shown in red (oxygen) and white (hydrogen). (b) The potential difference $\Delta\mathcal{V}_{\rm S}(x,y)$ (in Volts) from the three-dimensionally Gaussian smoothed charge density reveals that the polar and nonpolar portions of the surface polarize nearby water differently, enabling the mapping of surfaces with complex chemistries. (c) The characterization of this patterned surface provided by the solvation free energy of a hard cuboidal solute, $\beta\Delta\mu(x,y)$ (see text for details), illustrates that the electrostatics-based map is consistent with previous, water density fluctuation-based surface mapping techniques. A green diamond indicates the position of the hydroxyl group oxygen in (b) and (c).

(see the Appendix), the dipole and quadrupole in the case of water, and the potential difference across two phases in a slab geometry depends only on these two moments for nonionic systems[40,41]. However, this is true only in the special case of slab-like symmetry. Gaussian-smoothing over molecular length scales is critical for quantifying the electrostatic response to complex surfaces, where $\mathcal{V}_{\rm S}(\mathbf{r})$ is three-dimensional and has no apparent symmetry, as we discuss below.

III. CHARACTERIZATION OF CHEMICALLY PATTERNED SURFACES

The above analysis can be readily generalized to more complex, patterned surfaces with less symmetry. Here we show that the potential difference as a function of lateral position, $\Delta\mathcal{V}_{\rm S}(x,y)$, can be used to characterize the long-wavelength perturbations of the H-bond network induced by local changes in the chemical patterning of a planar molecular surface. Gaussian smoothing of the three-dimensional charge density in Eq. (2) ensures that relevant non-local perturbations of the water structure due to patterning of the surface in the xy-plane are captured, in addition to those in the z-direction, parallel to the surface normal

We first consider a purely hydrophobic (uncharged) silica surface, and add a single hydrophilic site, consisting of a hydrogen-bonding hydroxyl group[42,43], as shown in Figure 3a. A clear picture of the electrostatic response of water emerges upon examination of $\Delta\mathcal{V}_{\rm S}(x,y)$. Long-wavelength perturbations of the water H-bond network extending over roughly 10 Å in the plane of the surface are found when a single hydrophilic site is added to the

otherwise hydrophobic surface, Figure 3b. This is consistent with the concept that a single hydrophilic site can substantially pin water in its vicinity[21,43], and also is in accord with the results detailed above for homogeneous surfaces. As the number of hydrophilic sites is increased to three and seven sites, an increasingly larger region of water is perturbed, as illustrated in Figures 4a and 4b, respectively.

We also consider surfaces complementary to those in Figures 3 and 4, created by replacing hydrophilic groups with hydrophobic groups, and vice versa. For example, the complement of the surface in Figure 3a has a single apolar unit at the center of a surface covered in hydroxyl groups. The electrostatics-based maps for these hydrophilic surfaces with one, three, and seven hydrophobic sites are shown in Figure 5a, 5b, and 5c, respectively. Our findings are consistent with the idea that a hydrophobic site does not perturb the H-bond network near a hydrophilic surface nearly as much as a hydrophilic site does on an otherwise hydrophobic surface[21]. This can clearly be observed by comparing Figure 3b to Figure 5a, where a single hydrophobic site hardly perturbs the structure of water at the surface.

We additionally note that the response of water to a small hydrophobic patch on a hydrophilic surface is not equal to that above a uniform hydrophobic surface (a similar statement holds for the complementary surfaces). This equality becomes true for large enough patches, but the collective effects due to maintaining the H-bond network across the patch boundaries restricts the orientation of interfacial water molecules, and leads to larger values of $\Delta\mathcal{V}_{\rm S}(x,y)$ above these small patches than is expected from uniform surfaces with the same chemistry, see Figure 1d.

We further compare our electrostatics-based mapping procedure with a density fluctuation-based mapping in Figure 3c. The fluctuation maps shown here were generated by calculating the probability $P_v(N;x,y)$ of observing N water molecules in a probe volume $v = \sigma \times \sigma \times 4$ Å centered at the first peak of the nonuniform density of water at the surface for all x and y. The free energy of emptying this volume over the surface is then given by $\beta\Delta\mu(x,y) = -\ln P_v(0;x,y)$ and this is used to probe the relative hydrophobicity of the surface.

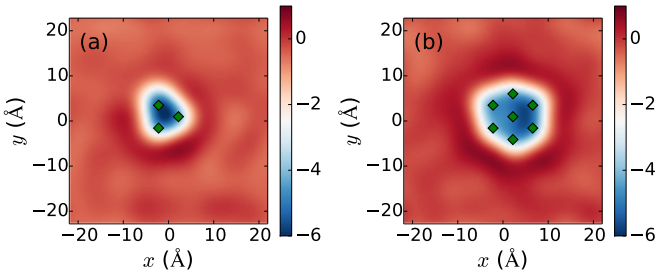


FIG. 4. Water molecules at the surface are significantly polarized when (a) three and (b) seven hydrophilic (hydroxyl) groups are added to an otherwise hydrophobic model silica surface, as indicated by the $\Delta\mathcal{V}_{\rm S}(x,y)$ plots shown here (in Volts). The positions of the hydroxyl group oxygen sites are indicated by the green diamonds.

This fluctuation-based mapping provides a description of interfacial water in accord with the electrostatics-based approach presented herein. For all surfaces studied here, consistency is found between the fluctuation-based and electrostatic-based maps of relative hydrophobicity.

Although both fluctuation-based and electrostatics-based maps discriminate well between hydrophobic and hydrophilic regions of a surface, the electrostatics-based mapping provides additional useful information about the polarization of water at the hydrophilic portions of the surface that standard fluctuations-based methods do not resolve. To illustrate this point, we construct a model surface with regions of differing polarity shown in Figure 6a. The first patch (red) has four surface units with $\xi = 1$, while the other two (blue) correspond to units with $\xi = -1$, one with three units and one with two. We expect that water in the vicinity of the surface will be polarized in opposite directions above the different dipolar units. The remainder of the surface is nonpolar (gray).

We find that $\Delta\mathcal{V}_{\rm S}(x,y)$ can readily distinguish between the regions of differing polarity. Water in the vicinity of the $\xi = 1$ patch responds in a manner that yields a positive $\Delta\mathcal{V}_{\rm S}$, while a negative $\Delta\mathcal{V}_{\rm S}$ is obtained over $\xi = -1$ regions. Surprisingly, the signs of these potentials are opposite to those obtained at uniform surfaces, stemming from the small size of the patches and the fact that most of the surface is apolar. Water molecules above the apolar surface do not penetrate into the grooves of the surface, as do waters near uniform $\xi = 1$ and $\xi = -1$ surfaces. Penetration of water into the surface grooves near the small patches in Figure 6a would lead to significant distortions of the hydrogen bond network, which are not compensated by these weakly hydrophilic patches. Instead, the orientation of water molecules in the vicinity of these patches is dominated by the tendency for their dipoles to align with the dipolar field of these patches.

This effect is due to the weakly hydrophilic nature of these artificial patches and the collective nature of the water hydrogen bond network. We expect a transition in $\Delta\mathcal{V}_{\rm S}$ with patch size, until the infinite limit shown in Figure 1d is reached. Indeed, differences in $\Delta\mathcal{V}_{\rm S}$ with patch size are already observed in moving from two to three dipolar units (top right to central blue patches in Figure 6a); the magnitude of $\Delta\mathcal{V}_{\rm S}$ increases. Such context-dependent behavior cannot be captured by focusing on the properties of the surface alone. In this case, surface-based mapping would predict no difference between these patches and the uniform surface because they have the same basic charges, despite the very different response of water based on the environment. These results provide a dramatic illustration of both the flexibility and subtlety of the nonlocal response of the hydrogen bond network to various perturbations, and the ability of the electrostatic maps to resolve their effects.

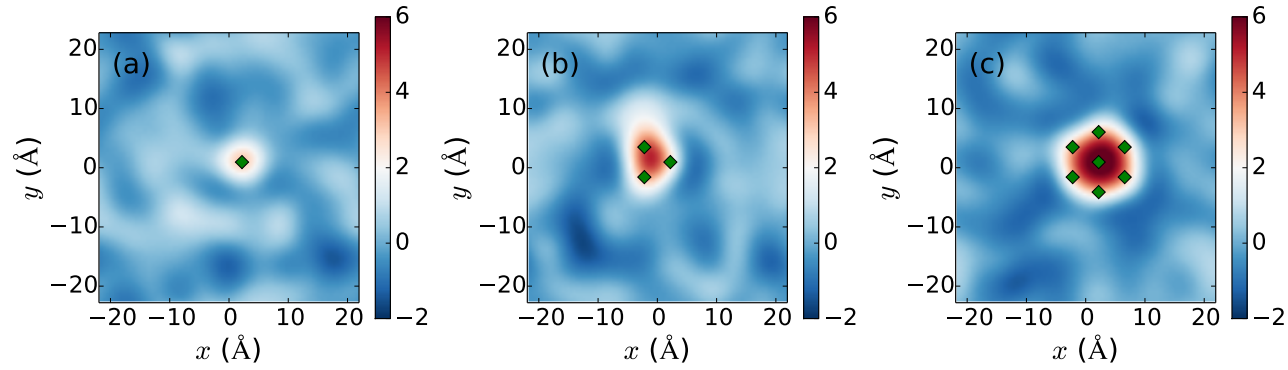


FIG. 5. The electrostatics-based mapping provided by $\Delta\mathcal{V}_S(x, y)$ (V) additionally provides a characterization of the response of water to hydrophilic silica surfaces with (a) one, (b) three, and (c) seven hydrophobic, apolar units, the positions of which are indicated by the diamonds.

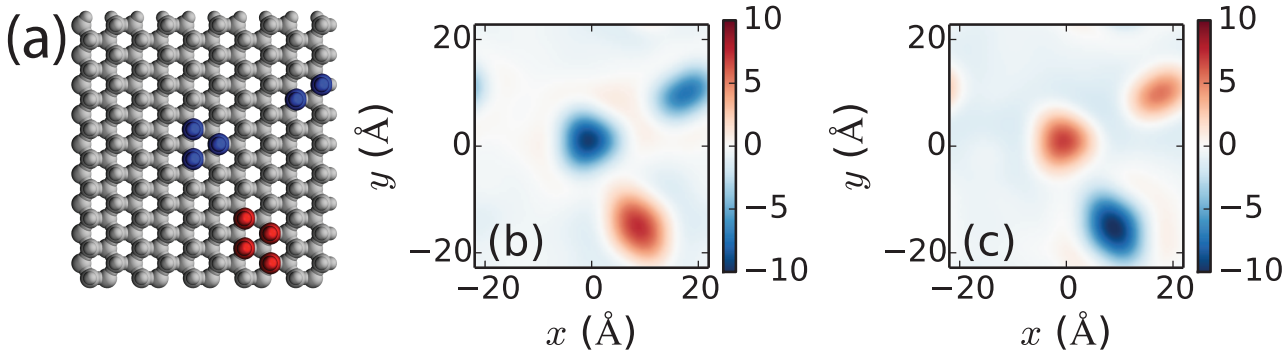


FIG. 6. (a) Snapshot of the model surface where the dipole moment of the surface units in the polar regions colored red and blue have opposite sign, while the rest of the surface is apolar (gray). (b) Potential difference $\Delta\mathcal{V}_S(x, y)$ due to the Gaussian-smoothed charge density above the patterned silica surface. (c) $\Delta\mathcal{V}_S(x, y)$ obtained above the inverse of the surface in panel (a), where the signs of the dipoles on the polar regions have been switched. Note that the opposite surface dipole moments induce differing responses in nearby water molecules, as captured by the smoothed electrostatic potential difference shown here.

We also consider the "inverse" of the surface in Figure 6a, which has the same pattern, but the signs of the dipoles are opposite to those of the surface in Figure 6a. Thus, we expect water in the vicinity of these patches to be polarized in the direction opposite to those of the inverse surface. Indeed, the electrostatic mapping described by $\Delta\mathcal{V}_S(x, y)$ demonstrates this to be true, as shown in 6c. This illustrates that the electrostatic mapping of interfaces readily uncovers the qualitatively different polarization of water at polar surface units, in addition to the relative hydrophobicity of regions of the surface.

IV. MAPPING PROTEIN SURFACES

The surface of the protein Hydrophobin II (HFBII) has both a hydrophilic and a hydrophobic region, allowing the protein to effectively act as a biomolecular Janus particle and assemble at hydrophobic-aqueous interfaces[44]. HFBII has been analyzed using classic hydrophobicity scales, in addition to the water density fluctuation-based techniques described in the Introduction[18,21]. The wide array of chemical and topographical complexities on the HFBII surface thus presents an ideal test case for extending the electrostatic mapping technique to protein surfaces.

In contrast to simple planar interfaces, one cannot generally define a vacuum region on the protein side of the protein-water interface. Instead, we can define a water-protein interface, $\mathbf{s}$, and evaluate the difference between the value of the long-ranged potential in the bulk and at this interface, $\Delta\mathcal{V}_S(\mathbf{s})$. This modified metric can still distinguish between regions of varying polarity, since our qualitative findings for planar interfaces would be unaltered by shifting the vacuum reference to the position of the interface ($z \approx 0$ Å in Figure 1 for example).

In the results shown here, we follow previous work[18] and evaluate $\Delta\mathcal{V}_S(\mathbf{s})$ at the Willard-Chandler smoothed interface defined by the protein heavy atoms alone[45]. We choose a low value of the density to define the interface, so that this surface envelopes the heavy atoms of the

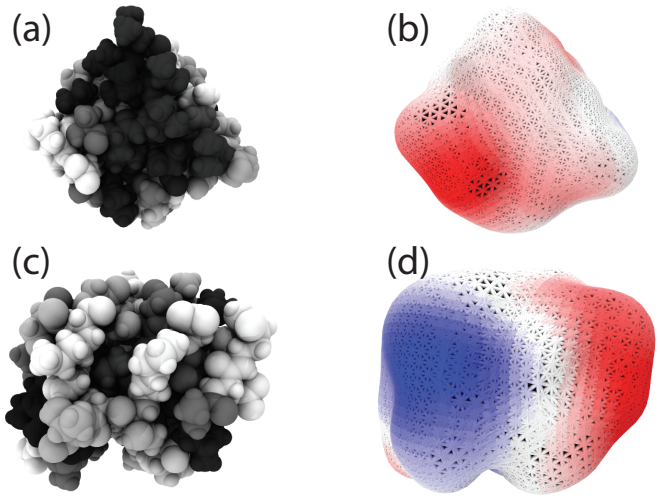


FIG. 7. (a,c) Two views of the Kyte-Doolittle residue-based mapping of Hydrophobin II (HFBII); increasing hydrophobicity coincides with the darkness of the residue. Panel (a) highlights large hydrophobic patch on the surface of the protein, while panel (c) focuses on hydrophilic regions. (b,d) The analogous two views of the electrostatic mapping of the water-HFBII interface. The protein surface as described by a Willard-Chandler smoothed interface for the protein heavy atoms is shown as a meshgrid and is colored by value of the $\Delta\mathcal{V}_S(\mathbf{s})$. Red represents negative values of the potential, blue indicates positive values of the potential, and white corresponds to values near zero, such that slightly negative, pale red/pink indicates values of the $\Delta\mathcal{V}_S$ observed above hydrophobic surfaces. Figures were made using VMD[46].

protein and is similar to a typical solvent excluded surface used commonly throughout the literature. As illustrated in Reference 30, because of the Gaussian smoothing in $\mathcal{V}_S(\mathbf{r})$, many molecular details in the protein substrate are unimportant. Thus the surface mapping procedure is rather insensitive to the precise definition of the protein-water interface, and many other reasonable choices could be made as well.

The electrostatics-based mapping of HFBII is compared to the classic Kyte-Doolittle hydrophobicity scale in Figure 7. The Kyte-Doolittle scale is indicated by the color of the residues in Figure 7a and 7b, such that hydrophobicity is proportional to the darkness of the residue color. The value of $\Delta\mathcal{V}_S(\mathbf{s})$ in Figure 7b and 7d is indicated by the color of the grid points on the mesh, which corresponds to the Willard-Chandler surface of the protein. The average interface is colored such that red represents large negative values of $\Delta\mathcal{V}_S(\mathbf{s})$, blue indicates large positive values of the potential, and white corresponds to values near zero. With this scaling, values of $\Delta\mathcal{V}_S(\mathbf{s})$ indicative of hydrophobic surfaces are colored pink/pale red.

The electrostatic mapping procedure readily uncovers the large hydrophobic patch of HFBII shown in Figure 7a and 7b. The value of $\Delta\mathcal{V}_S(\mathbf{s})$ in the region of this patch is consistent with that for a hydrophobic surface. However, note that there is a highly hydrophilic group at the edge of this hydrophobic patch (bottom left, red region). The polarization caused by this patch does not dissipate instantly, and the size of the hydrophobic patch is predicted to be smaller than that from surface-based scales. This agrees rather well with findings of other water-based characterizations of HBFII[18,21].

As was detailed in the previous section, polar surfaces can polarize water in opposing directions. The maps of HFBII indicate the formation of such patterns in a biological context. The blue (positive $\Delta\mathcal{V}_S(\mathbf{s})$) portion of the map in Figure 7b is dominated by the response of water molecules to the positively charged lysine residue in the region. Analogously, the red (negative $\Delta\mathcal{V}_S(\mathbf{s})$) region on the right of Figure 7b describes the response of water to a negatively charged aspartic acid residue. The identification of such hydrophilic regions of differing polarity may be crucial to understanding the binding of biomolecules. For example, these oppositely charged residues come into close contact with those of neighboring HFBII molecules when forming multimeric assemblies[47], and a characterization of the polarization of water near polar regions of proteins may help predict their involvement in biomolecular interactions[48].

V. CONCLUSIONS

In this work, we have introduced a novel electrostatics-based method for characterizing the long-wavelength, collective response of water to complex surfaces. This approach effectively coarse-grains over molecular scale details in order to uncover the underlying electrostatic behavior of the system, enabling one to distinguish larger scale rearrangements of the hydrogen bond network of water at an interface and consequently differentiate hydrophobic and hydrophilic surfaces. This approach is quite efficient computationally, requiring only a single equilibrium simulation of a complex surface in explicit water.

In addition to distinguishing between hydrophobic and hydrophilic regions, the approach introduced here can further distinguish the relative polarization of water in response to hydrophilic groups. An understanding of the relative polarization of water at surfaces is important for a range of processes, including understanding and predicting ion adsorption to biomolecular interfaces. It has been postulated that the sign of the surface potential can drive ions to adsorb to interfaces, at least in classical models[49]. As such, if adsorption were to be favorable at a patterned surface like that in Figure 6, for example, one might expect that ions of opposite sign would adsorb to regions of opposite dipole moments.

Differentiating the relative polarity of water in interfacial regions may also be useful in the description of binding processes in general. In particular, it seems plausible that polarization-based hydration repulsion could occur between two surfaces[50,51]. For example, consider placing

in close proximity two surfaces that have maps like those in Figure 6b, such that the blue regions align. As the two surfaces are brought closer together, polarized interfacial water may "interfere deconstructively" and effectively repel the two surfaces, because the hydrogen bond network is polarized in different directions everywhere but the midpoint between the interfaces, where the polarization must vanish by symmetry[50,51]. Therefore, to achieve small interplate distances, confined water must be (unfavorably) depolarized.

In contrast, one might expect that bringing together surfaces with regions of opposing polarity, like the red and blue regions in Figure 6, would instead lead to hydrogen bond networks that interfere *constructively*, because the inter-surface water is polarized in the same direction everywhere between these patches. In this case, unfavorable depolarization may not occur, minimizing this contribution to the effective repulsion between surfaces and possibly leading to an effective attraction between hydrophilic surfaces[51,52].

However, in more general cases of molecular assembly, the polarization of water molecules, and therefore $\Delta\mathcal{V}_{\rm S}(\mathbf{r})$, depends on a multitude of parameters including the separation and relative orientation of the confining surfaces, and more than bulk equilibrium simulations of individual surfaces are required for a quantitatively accurate description of such phenomena. Nevertheless, the electrostatic mapping described herein should provide qualitative insight into many relevant features of solvent polarization effects needed to understand hydration mediated forces.

VI. METHODS

A. Simulation of Silica Surfaces

All simulations of water near model silica surfaces were performed using a modified version of the DL_POLY software package (version 2.18)[53], following the work of Hu and Weeks[54]. Simulation cells $45.6 \times 43.9 \times 180$ Å^3 in volume were used to simulate 2468 SPC/E[55] water molecules at model silica surfaces with a buffering liquid-vapor interface far from the surface, to maintain a constant coexistence pressure while in the canonical ensemble (The large size of the cell in the z-dimension is also useful for evaluating electrostatics in slab like geometries.). A temperature of 298 K was maintained using a Berendsen thermostat[56]. Lennard-Jones interactions were truncated and shifted at a distance of 11 Å. The slab corrected Ewald summation method of Yeh and Berkowitz[57] was used to handle the evaluation of electrostatic interactions, with a real space cutoff of 11 Å, switching parameter $\alpha = 0.3$ Å^{-1}, and a maximum number of k-space vectors of $k_x = 10$, $k_y = 10$, and $k_z = 30$ in the $x-$, $y-$, and $z-$directions, respectively, such that the k-space sums run from $-k_x$ to k_x, for example. For the patterned dipolar surfaces discussed in Figure 6, a larger number of k-vectors is needed, such that $k_x = 20$, $k_y = 20$, and $k_z = 30$ for these simulations.

B. Protein Simulation

Simulations of HFBII (PDB ID: 2B97)[44] in SPC/E[55] water were performed using the GROMACS 4.5.3 software package[58] and the AMBER 94 force field[59], following the work of Patel and Garde[18]. As with the silica surfaces, simulations were performed in the presence of a buffering liquid-vapor interface, now with one in each z-direction. The protein atoms were held fixed at the center of the liquid slab. Production simulations used for analysis totaled 6 ns in length, and a constant temperature of 300 K was maintained using the canonical velocity rescaling algorithm[60]. All Lennard-Jones interactions were truncated at a distance of 10 Å, and long-ranged corrections to the energy and pressure were ignored. Electrostatic interactions were evaluated using the particle mesh Ewald method[61].

ACKNOWLEDGMENTS

This work was supported by the National Science Foundation (Grants CHE0848574 and CHE1300993). We are grateful to Jocelyn Rodgers for helpful discussions. RCR also acknowledges Amish Patel for stimulating discussions and Erte Xi for assistance with the generation of the protein interface.

Appendix A: Multipole Moment Expansion of Gaussian-Smoothed Charge Densities

Here, we present the multipole expansion for the Gaussian-smoothed charge density, $\rho^{q\sigma}(\mathbf{r})$, and how it relates to that of the bare charge density $\rho^{q}(\mathbf{r})$. For generality, we consider the interaction energy between two d-dimensional Gaussian-smoothed charge densities, with centers $\mathbf{r}_i$ and $\mathbf{r}_j$, where the position vector is defined by

$$\mathbf{r} = (x_1, x_2, ..., x_d)\,, \tag{A1}$$

and $d \in \mathbb{N}$. We consider the interaction energy of the two charge distributions under consideration, $\rho_i^{q\sigma}(\mathbf{r}_i)$ and $\rho_j^{q\sigma}(\mathbf{r}_j)$, respectively, to be of the form

$$w(\mathbf{r}_{ij}) = \int d\mathbf{r} \int d\mathbf{r}' \rho_i^{q\sigma}(\mathbf{r}-\mathbf{r}_i)\rho_j^{q\sigma}(\mathbf{r}'-\mathbf{r}_j)\frac{1}{\epsilon\,|\mathbf{r}-\mathbf{r}'|}, \tag{A2}$$

where we use the 3-dimensional Coulomb potential. However, the multipoles themselves depend only on the dimensionality of the charge density, and the relationship between the multipoles of the bare and smoothed charge densities described below are independent of the form of

the potential. This interaction energy can be rewritten as a $\mathbf{k}$-space integral,

$$w(\mathbf{r}_{ij}) = \frac{1}{(2\pi)^d}\int d\mathbf{k}\hat{\rho}_i^{q\sigma}(-\mathbf{k})\hat{\rho}_j^{q\sigma}(\mathbf{k})e^{-i\mathbf{k}\cdot\mathbf{r}_{ij}}\frac{4\pi}{\epsilon k^2}, \quad \text{(A3)}$$

where we have defined the d-dimensional Fourier transform and inverse Fourier transform of a function f as

$$\hat{f}(\mathbf{k}) = \int d\mathbf{r}e^{-i\mathbf{k}\cdot\mathbf{r}}f(r)$$

and

$$f(\mathbf{r}) = \frac{1}{(2\pi)^d}\int d\mathbf{k}e^{i\mathbf{k}\cdot\mathbf{r}}\hat{f}(\mathbf{k}),$$

respectively.

Now to examine the asymptotic behavior as $k \to 0$, we Tayor expand the smoothed charge densities about $k = 0$, such that

$$\hat{\rho}_i^{q\sigma}(\mathbf{k}) = \sum_{n_i}\frac{1}{n_i!}\mathbf{k}^{n_i}\cdot\nabla_{\mathbf{k}}^{n_i}\hat{\rho}_i^{q\sigma}(0), \quad \text{(A4)}$$

where $\nabla_{\mathbf{k}}$ is the d-dimensional gradient with respect to $\mathbf{k}$. We can then insert A4 into A3 to obtain

$$w(\mathbf{r}_{ij}) = \sum_{n_i,n_j}\frac{1}{n_i!n_j!}\left[\nabla_{\mathbf{k}}^{n_i}\hat{\rho}_i^{q\sigma}(0)\cdot(-i\nabla_{\mathbf{r}})^{n_i}\right] \cdot\left[\nabla_{\mathbf{k}}^{n_j}\hat{\rho}_j^{q\sigma}(0)\cdot(i\nabla_{\mathbf{r}})^{n_j}\right]\frac{1}{\epsilon r} \quad \text{(A5)}$$

Now, we can define

$$\frac{i^{n_i}}{n_i!}\nabla_{\mathbf{k}}^{n_i}\hat{\rho}_i^{q\sigma}(0) \equiv \mathcal{M}_i^{\sigma}(n_i), \quad \text{(A6)}$$

such that

$$\mathcal{M}_i^{\sigma}(n_i) = \frac{1}{n_i!}\int d\mathbf{r}\rho_i^{q\sigma}(\mathbf{r})\mathbf{r}^{n_i}, \quad \text{(A7)}$$

and $\mathcal{M}^{\sigma}(n)$ is the nth multipole moment of the smoothed charge distribution. Finally, we can rewrite A5 as

$$w(\mathbf{r}_{ij}) = \sum_{n_i,n_j}\left[\mathcal{M}_i^{\sigma}(n_i)\cdot(-\nabla_{\mathbf{r}})^{n_i}\right]\cdot\left[\mathcal{M}_j^{\sigma}(n_j)\cdot\nabla_{\mathbf{r}}^{n_j}\right]\frac{1}{\epsilon r} \quad \text{(A8)}$$

so that the energy is now expressed in terms of the multipole moments of the smoothed charge distributions.

One may then inquire into how these multipole moments relate to those of the bare charge densities, $\rho^q(\mathbf{r})$. In order to relate the two sets of multipoles, we first consider the Fourier transform of the smoothed charge density, which, using the convolution theorem, can be written as

$$\hat{\rho}^{q\sigma}(\mathbf{k}) = \hat{\rho}^q(\mathbf{k})\hat{\rho}_G(\mathbf{k}), \quad \text{(A9)}$$

where

$$\hat{\rho}_G(\mathbf{k}) = e^{-\frac{k^2\sigma^2}{4}}. \quad \text{(A10)}$$

In general, the nth order multipole moment $\mathcal{M}^{\sigma}(n)$ is given by

$$\mathcal{M}^{\sigma}(n) = \frac{i^n}{n!}\sum_{m=0}^{n}\binom{n}{m}\hat{\rho}^{q(n-m)}(0)\otimes\hat{\rho}_G^{(m)}(0), \quad \text{(A11)}$$

where $\hat{f}^{(n)}(0) = \left[\nabla_{\mathbf{k}}^n\hat{f}(\mathbf{k})\right]\Big|_{k=0}$ is a tensor of rank n, $\otimes$ indicates a symmetric outer product, and

$$\binom{n}{m} = \frac{n!}{m!(n-m)!}$$

is the binomial coefficient. The gradients of the $\mathbf{k}$-space Gaussian function are given by

$$\hat{\rho}_G^{(n)}(\mathbf{k}) = (-1)^n e^{-k^2\sigma^2/4}\mathbf{H}_n\left(\frac{\mathbf{k}\sigma}{2}\right), \quad \text{(A12)}$$

such that $\mathbf{H}_n(a\mathbf{x})$ is a rank n tensor-analog of the Hermite functions with elements

$$H_{ij\cdots v}(a\mathbf{x};n) = (-1)^n e^{a^2\mathbf{x}^2}\frac{\partial^n}{\partial x_i\partial x_j\cdots\partial x_v}\left(e^{-a^2\mathbf{x}^2}\right), \quad \text{(A13)}$$

where a is a constant and $\mathbf{x} = (x_1, x_2, ..., x_d)$ is a general d-dimensional vector.

All odd derivatives of $\hat{\rho}_G(\mathbf{k})$ will vanish at $k = 0$ due to symmetry, therefore, we can rewrite A11 as

$$\mathcal{M}^{\sigma}(n) = \frac{i^n}{n!}\sum_{\substack{m=0\\ m\in\mathbb{E}}}^{n}(-1)^m\binom{n}{m}\hat{\rho}^{q(n-m)}(0)\otimes\mathbf{A}_m\left(\frac{\sigma}{2}\right), \quad \text{(A14)}$$

where $\mathbf{A}_m(a) \equiv \left[\mathbf{H}_m(a\mathbf{k})\right]\big|_{k=0}$ and $\mathbb{E}$ is the set of even whole numbers.

Equation A14 can be written in the equivalent form

$$\mathcal{M}^{\sigma}(n) = \mathcal{M}(n) + \sum_{\substack{m=2\\ m\in\mathbb{E}}}^{n}\frac{(-1)^m i^m}{m!}\mathcal{M}(n-m)\otimes\mathbf{A}_m\left(\frac{\sigma}{2}\right), \quad \text{(A15)}$$

making the relation between $\mathcal{M}^{\sigma}(n)$ and $\mathcal{M}(n)$ apparent. Therefore, in order for $\mathcal{M}^{\sigma}(n) = \mathcal{M}(n)$ to hold, where $\mathcal{M}(n)$ is the nth multipole moment of the bare charge distribution ρ^q, all multipoles of the bare charge density ρ^q of order less than $n-1$ and of even (odd) order, for n even (odd), must be identically zero,

$$\mathcal{M}^{\sigma}(n) = \mathcal{M}(n) \iff \mathcal{M}(s) = 0\ \forall\ s = n-l, \quad \text{(A16)}$$

where

$$l = \begin{cases} 2,4,6,...,n; \text{ for } n \text{ even} \\ 2,4,6,...,n-1; \text{ for } n \text{ odd.} \end{cases} \quad \text{(A17)}$$

To illustrate this condition, we present the first few multipole moments of the Gaussian-smoothed charge density. The monopole moment of $\rho^{q\sigma}$ is trivially given by $\mathcal{M}^{\sigma}(0) = \mathcal{M}(0)$, and note that for neutral charge

distributions the monopole moment is zero. The dipole moment, $n = 1$, is also trivially given by

$$\mathcal{M}^\sigma(1) = \mathcal{M}(1),$$

illustrating that the dipole moment of ρ^q is conserved upon Gaussian-smoothing. In addition, the quadrupole moment is given by

$$\begin{aligned}\mathcal{M}^\sigma(2) &= \mathcal{M}(2) - \frac{1}{2}\mathcal{M}(0) \otimes \mathbf{A}_2\left(\frac{\sigma}{2}\right) \\ &= \mathcal{M}(2) + \frac{\sigma^2}{4}\mathcal{M}(0)\mathbf{I}_3, \end{aligned} \tag{A18}$$

while the Gaussian smoothed octupole is similarly given by

$$\mathcal{M}^\sigma(3) = \mathcal{M}(3) + \frac{\sigma^2}{4}\mathcal{M}(1) \otimes \mathbf{I}_3, \tag{A19}$$

where $\mathbf{I}_n$ is the $n \times n$ identity matrix. For neutral charge distributions, like non-ionic molecular charge distributions (water), both the dipole *and* quadrupole moments are conserved upon Gaussian-smoothing, but not higher order moments. From the work of Wilson and Pratt[40], it follows that only the potential difference across two phases in a slab-like geometry is conserved upon Gaussian-smoothing of the charge density (or the potential), because this depends only on the dipole and quadrupole moments of a molecular fluid. However, contrary to a previous report[62], $\mathcal{V}_\mathrm{S}(z) \neq \mathcal{V}(z)$, because higher order multipoles are modified by smoothing.

[1] M. J. Solomon, "Directions for targeted self-assembly of anisotropic colloids from statistical thermodynamics," Curr. Opin. Coll. Int. Sci, **16**, 158 (2011).

[2] F. B. Sheinerman, R. Norel, and B. Honig, "Electrostatic aspects of protein-protein interactions," Curr Opin Struct Biol, **10**, 153 (2000).

[3] K. J. M. Bishop, C. E. Wilmer, S. Soh, and B. A. Grzybowski, "Nanoscale forces and their uses in self-assembly," Small, **5**, 1600 (2009).

[4] G. M. Whitesides and B. Grzybowski, "Self-assembly at all scales," Science, **295**, 2418 (2002).

[5] B. J. Berne, J. D. Weeks, and R. Zhou, "Dewetting and hyrophobic interactions in physical and biological systems," Annu. Rev. Phys. Chem., **60**, 85 (2009).

[6] D. Chandler, "Interfaces and the driving force of hydrophobic assembly," Nature, **437**, 640 (2005).

[7] K. A. Dill, "Dominant forces in protein folding," Biochemistry, **29**, 7133 (1990).

[8] C. M. Dobson, "Protein folding and misfolding," Nature, **426**, 884 (2003).

[9] L. Mirny and E. Shaknovich, "Protein folding theory: From lattice to all-atom models," Annu. Rev. Biophys. Biomol. Struct., **30**, 361 (2001).

[10] D. Thirumalai, E. P. O'Brien, G. Morrison, and C. Hyeon, "Theoretical perspectives on protein folding," Annu Rev Biophys, **39**, 159 (2010).

[11] S. Jones and J. M. Thornton, "Principles of protein-protein interactions," Proc. Natl. Acad. Sci. U.S.A., **93**, 13 (1996).

[12] W. L. DeLano, "Unraveling hot spots in binding interfaces: progress and challenges," Curr Opin Struct Biol, **12**, 14 (2002).

[13] J. Kyte and R. F. Doolittle, "A simple method for displaying the hydropathic character of a protein," J Mol Biol, **157**, 105 (1982).

[14] R. Zhou, B. D. Silverman, A. K. Royyuru, and P. Athma, "Spatial profiling of protein hydrophobicity: Native vs. decoy structures," Proteins: Struct. Funct. Bioinform., **52**, 561 (2003).

[15] L. Hua, X. Huang, P. Liu, R. Zhou, and B. J. Berne, "Nanoscale dewetting transition in protein complex folding," J. Phys. Chem. B, **111**, 9069 (2007).

[16] L. H. Kapcha and P. J. Rossky, "A simple atomic-level hydrophobicity scale reveals protein interfacial structure," J. Mol. Biol., **426**, 484 (2014).

[17] R. Godawat, S. N. Jamadagni, and S. Garde, "Characterizing hydrophobicity of interfaces by using cavity formation, solute binding, and water correlations," Proc. Natl. Acad. Sci. U.S.A., **106**, 15119 (2009).

[18] A. J. Patel and S. Garde, "Efficient method to characterize the context-dependent hydrophobicity of proteins," J. Phys. Chem. B, **118**, 1564 (2014).

[19] A. J. Patel, P. Varilly, S. N. Jamadagni, H. Acharya, S. Garde, and D. Chandler, "Extended surfaces modulate hydrophobic interactions of neighboring solutes," Proc. Natl. Acad. Sci. U.S.A., **108**, 17678 (2011).

[20] S. N. Jamadagni, R. Godawat, and S. Garde, "Hydrophobicity of proteins and interfaces: Insights from density fluctuations," Ann. Rev. Chem. Biomol. Engg., **2**, 147 (2011).

[21] H. Acharya, S. Vembanur, S. N. Jamadagni, and S. Garde, "Mapping hydrophobicity at the nanoscale: Applications to heterogeneous surfaces and proteins," Faraday Discuss., **146**, 353 (2010).

[22] A. J. Patel, P. Varilly, D. Chandler, and S. Garde, "Quantifying density fluctuations in volumes of all shapes and sizes using indirect umbrella sampling," J. Stat. Phys., **145**, 265 (2011).

[23] A. J. Patel, P. Varilly, S. N. Jamadagni, M. F. Hagan, D. Chandler, and S. Garde, "Sitting at the edge: How biomolecules use hydrophobicity to tune their interactions and function," J. Phys. Chem. B, **116**, 2498 (2012).

[24] B. Widom, "Some topics in the theory of fluids," J. Chem. Phys., **39**, 2808 (1963).

[25] G. Hummer, S. Garde, A. E. García, A. Pohorille, and L. R. Pratt, "An information theory model of hydrophobic interactions," Proc. Natl. Acad. Sci. USA, **93**, 8951 (1996).

[26] S. Garde, G. Hummer, A. E. García, M. E. Paulaitis, and L. R. Pratt, "Origin of entropy convergence in hydrophobic hydration and protein folding," Phys. Rev. Lett., **77**, 4966 (1996).

[27] T. L. Beck, M. E. Paulaitis, and L. R. Pratt, *The Potential Distirbution Theorem and Models of Molecular Solutions* (Cambridge University Press, 2006).

[28] N. Giovambattista, P. G. Debenedetti, and P. J. Rossky, "Enhanced surface hydrophobicity by coupling of surface polarity and topography," Proc. Natl. Acad. Sci. USA, **106**, 15181 (2009).

[29] N. Giovambattista, P. G. Debenedetti, and P. J. Rossky, "Correction for "enhanced surface hydrophobicity by coupling of surface polarity and topography"," Proc. Natl. Acad. Sci. USA, **110**, 6608 (2013).

[30] J. M. Rodgers and J. D. Weeks, "Local molecular field theory for the treatment of electrostatics," J. Phys.: Condens. Matter, **20**, 494206 (2008).

[31] J. M. Rodgers and J. D. Weeks, "Interplay of local hydrogen-bonding and long-ranged dipolar forces in simulations of confined water," Proc. Natl. Acad. Sci. USA, **105**, 19136 (2008).

[32] J. M. Rodgers, Z. Hu, and J. D. Weeks, "On the efficient and accurate short-ranged simulations of uniform polar molecular liquids," Mol. Phys., **109**, 1195 (2011).

[33] J. D. Jackson, *Classical Electrodynamics* (John Wiley & Sons, 1999).

[34] A. Zangwill, *Modern Electrodynamics* (Cambridge University Press, 2013).

[35] S. H. Lee and P. J. Rossky, "A comparison of the structure and dynamics of liquid water at hydrophobic and hydrophilic surfaces – a molecular dynamics simulation study," J. Chem. Phys., **100**, 3334 (1994).

[36] C. Y. Lee, J. A. McCammon, and P. J. Rossky, "The structure

of liquid water at an extended hydrophobic surface," J. Chem. Phys., **80**, 4448 (1984).
[37]T. G. Trudeau, K. C. Jena, and D. K. Hore, "Water structure at solid surfaces of varying hydrophobicity," J. Phys. Chem. C, **113**, 20002 (2009).
[38]R. C. Remsing, M. D. Baer, G. K. Schenter, C. J. Mundy, and J. D. Weeks, "The role of broken symmetry in solvation of a spherical cavity in classical and quantum water models," J. Phys. Chem. Lett., **5**, 2767 (2014).
[39]A. P. Willard and D. Chandler, "The molecular structure of the interface between water and a hydrophobic substrate is liquid-vapor like," J. Chem. Phys., **141**, 18C519 (2014).
[40]M. A. Wilson, A. Pohorille, and L. R. Pratt, "Comment on "study on the liquid-vaport interface of water. i. simulation results of thermodynamics properties and orientational structure"," J. Chem. Phys., **90**, 5211 (1989).
[41]L. R. Pratt, "Contact potentials of solution interfaces: Phase equilibrium and interfacial electric fields," J. Phys. Chem., **96**, 25 (1992).
[42]N. Giovambattista, P. J. Rossky, and P. G. Debenedetti, "Effect of pressure on the phase behavior and structure of water confined between nanoscale hydrophobic and hydrophilic plates," Phys. Rev. E, **73**, 041604 (2006).
[43]N. Giovambattista, P. G. Debenedetti, and P. J. Rossky, "Hydration behavior under confinement by nanoscale surfaces with patterned hydrophobicity and hydrophilicity," J. Phys. Chem. C, **111**, 1323 (2007).
[44]J. Hakanpää, M. Linder, A. Popov, A. Schmidt, and J. Rouvinen, "Hydrophobin hfbii in detail: ultrahigh-resolution structure at 0.75 a," Acta Crystallogr D Biol Crystallogr, **62**, 356 (2006).
[45]A. P. Willard and D. Chandler, "Instantaneous liquid interfaces," J. Phys. Chem. B, **114**, 1954 (2010).
[46]W. Humphrey, A. Dalke, and K. Schulten, "VMD – Visual Molecular Dynamics," Journal of Molecular Graphics, **14**, 33 (1996).
[47]J. Hakanpää, G. R. Szilvay, H. Kaljunen, M. Maksimainen, M. Linder, and J. Rouvinen, "Two crystal structures of trichoderma reesei hydrophobin hfbi–the structure of a protein amphiphile with and without detergent interaction," Protein Sci, **15**, 2129 (2006).
[48]F. B. Sheinerman, R. Norel, and B. Honig, "Electrostatic aspects of protein-protein interactions," Curr Opin Struct Biol, **10**, 153 (2000).
[49]M. D. Baer, A. C. Stern, Y. Levin, D. J. Tobias, and C. J. Mundy, "Electrochemical surface potential due to classical point charge models drives anion adsorption to the air-water interface," J. Phys. Chem. Lett., **3**, 1565 (2012).
[50]E. Schneck, F. Sedlmeier, and R. R. Netz, "Hydration repulsion between biomembranes results from an interplay of dehydration and depolarization," Proc Natl Acad Sci U S A, **109**, 14405 (2012).
[51]M. Kanduč, A. Schlaich, E. Schneck, and R. R. Netz, "Hydration repulsion between membranes and polar surfaces: Simulation approaches versus continuum theories," Adv. Colloid Interface Sci., **208**, 142 (2014).
[52]M. Kanduč, E. Schneck, and R. R. Netz, "Attraction between hydrated hydrophilic surfaces," Chem. Phys. Lett., **610–611**, 375 (2014).
[53]W. Smith, C. Yong, and P. Rodger, "DL_POLY: Application to molecular simulation," Mol. Simul., **28**, 385 (2002).
[54]Z. Hu and J. D. Weeks, "Acetonitrile on silica surfaces and at its liquid-vapor interface: Structural correlations and collective dynamics," J. Phys. Chem. C, **114**, 10202 (2010).
[55]H. J. C. Berendsen, J. R. Grigera, and T. P. Straatsma, "The missing term in effective pair potentials," J. Phys. Chem., **91**, 6269 (1987).
[56]H. J. C. Berendsen, J. P. M. Postma, W. F. van Gunsteren, A. DiNiola, and J. R. Haak, "Molecular dynamics with coupling to an external bath," J. Chem. Phys., **81**, 3684 (1984).
[57]I. C. Yeh and M. L. Berkowitz, "Ewald summation for systems with slab geometry," J. Chem. Phys., **111**, 3155 (1999).
[58]B. Hess, C. Kutzner, D. van der Spoel, and E. Lindahl, "Gromacs 4: Algorithms for highly efficient, load-balanced, and scalable molecular simulation," J. Chem. Theory Comp., 435 (2008).
[59]W. D. Cornell, P. Cieplak, C. I. Bayly, I. R. Gould, K. M. Merz, D. M. Ferguson, D. C. Spellmeyer, T. Fox, J. W. Caldwell, and P. A. Kollman, "A second generation force field for the simulation of proteins, nucleic acids, and organic molecules," J. Am. Chem. Soc., **117**, 5179 (1995), http://pubs.acs.org/doi/pdf/10.1021/ja00124a002.
[60]G. Bussi, D. Donadio, and M. Parrinello, "Canonical sampling through velocity rescaling," J. Chem. Phys., **126**, 014101 (2007).
[61]U. Essmann, L. Perera, M. L. Berkowitz, T. Darden, H. Lee, and L. G. Pedersen, "A smooth particle mesh ewald method," J. Chem. Phys., **103**, 8577 (1995).
[62]I. Vorobyov and T. W. Allen, "The electrostatics of solvent and membrane interfaces and the role of electronic polarizability." J. Chem. Phys., **132**, 185101 (2010).